Indian Journal of Geo Marine Sciences
Vol. 54 (06), June 2025, pp. 277-284
DOI: 10.56042/ijms.v54i06.13689

Research Article

Comparison of vegetation indices derived from a consumer-grade UAV and the Google Earth Engine platform for seasonal mangrove canopy assessment

L Valderrama-Landeros[a], F Flores-de-Santiago*[,b], R Rodríguez-Sobreyra[b] & F Flores-Verdugo[c]

[a]Subcoordinación de Percepción Remota, Comisión Nacional Para el Conocimiento y Uso de la Biodiversidad (CONABIO), Mexico City 14010, Mexico

[b]Unidad Académica Procesos Oceánicos y Costeros, Instituto de Ciencias del Mar y Limnología, Universidad Nacional Autónoma de México, Mexico City 04510, Mexico

[c]Unidad Académica Mazatlán, Instituto de Ciencias del Mar y Limnología, Universidad Nacional Autónoma de México, Mazatlán 82040, Mexico

*[E-mail: ffloresd@cmarl.unam.mx]

Received 11 September 2024; revised 23 April 2025

Mangrove forests, though classified as evergreen vegetation, exhibit substantial year-round litterfall, necessitating species-level phenological understanding for accurate remote sensing classification. This study compared monthly phenological variations across four mangrove classes *viz.*, red (*Rhizophora mangle*), white (*Laguncularia racemosa*), and black mangrove (*Avicennia germinans*) in both shrub and fringe conditions, using consumer-grade UAV data and Sentinel-2 imagery from Google Earth Engine (GEE) over a 15-month period. Visible (RGB) data from UAV orthomosaics and Sentinel-2 were analysed using four RGB-vegetation indices, revealing similar temporal trends between platforms, though with consistently lower intensity values in UAV-derived data. Notably, the weakest correlations occurred in *Rhizophora mangle* and the shrub *Avicennia germinans* classes. These findings demonstrate UAVs´ potential for high-resolution phenological monitoring where spaceborne sensors lack sufficient resolution, while highlighting species-specific limitations for mangrove forest assessments.

[**Keywords**: Forested wetland, Mexico, Sentinel-2, Visible indices]

Introduction

Mangrove forests are coastal wetlands found in tropical and subtropical regions[1]. These highly productive ecosystems sequester significant amounts of carbon as biomass and provide organic nutrients for marine fauna[2]. Mangroves play a crucial role in maintaining the ecological balance of adjacent aquatic ecosystems, such as seagrass beds and coral reefs[3]. Additionally, they support local communities through ecosystem services, including coastal protection and fisheries of economic importance[4]. Given that mangrove species exhibit distinct responses to environmental disturbances, comprehensive assessments of their seasonal species composition and spatial distribution are essential for effective global management of these vital coastal habitats[5].

Mangrove forests present substantial challenges for fieldwork due to their waterlogged, soft-sediment substrates and hypersaline conditions[5]. As a result, remote sensing has become an increasingly vital tool for mapping and monitoring mangroves across large, inaccessible regions[6]. However, traditional medium-resolution satellite imagery often fails to accurately differentiate mangrove species, underscoring the need for higher-resolution technologies[7]. Additionally, classifying mangrove species remains difficult due to the phenological variations influenced by pigment content (*e.g.*, chlorophyll), ambient temperature, freshwater availability, and soil salinity, particularly in arid regions[8].

The scarcity of phenology-based assessments for mangrove species is largely due to the lack of continuous, high-temporal-resolution spatial data[9]. However, the Sentinel-2 multispectral sensor now enables satellite data acquisition at 10-meter spatial resolution and a revisit time of 2 – 5 days[10], offering superior capability for detailed phenological monitoring of mangrove species compared to traditional platforms like Landsat (30-meter spatial resolution, 16-day revisit time)[11]. Furthermore, the cloud-based Google Earth Engine (GEE) platform facilitates large-scale processing of satellite data,

offering researchers in geospatial and phenology studies a powerful tool for rapid analysis[9].

Recent advancements in Unmanned/Unoccupied Aerial Vehicle (UAV) technology have enabled ultra-high spatial resolution remote sensing of mangrove species at the centimetre-scale level[12]. With declining costs of UAV platforms and sensors, coupled with improved data processing software, UAVs now provide greater flexibility than traditional piloted airborne systems or satellite-based approaches[13]. The growing utility of UAVs is clear from the sharp rise in related research publications over the past three decades[14]. However, while most UAV applications have focused on precision agriculture, few studies have explored their potential for seasonal mangrove assessments[15]. Therefore, this study aimed to compare time-series vegetation index profiles derived from a consumer-grade UAV camera with harmonic analyses of GEE satellite data.

Materials and Methods

Study area

The Urias coastal lagoon system (Fig. 1a) is an 18 km^2 shallow, saline, vertically mixed water body located on an alluvial plain in southern Sinaloa, Mexico. This subtropical semiarid ecosystem experiences mean annual temperatures of 24 – 26 °C and receives 800 – 1000 mm of seasonal rainfall (July – September). Directly connected to the Pacific Ocean, via tidal channels, the coastal lagoon exhibits semi-diurnal tides (max amplitude 1.8 m) with spring tides occurring during the summer (June – September). The system comprises tidal creeks, seasonal floodplains, hypersaline saltpans, and a

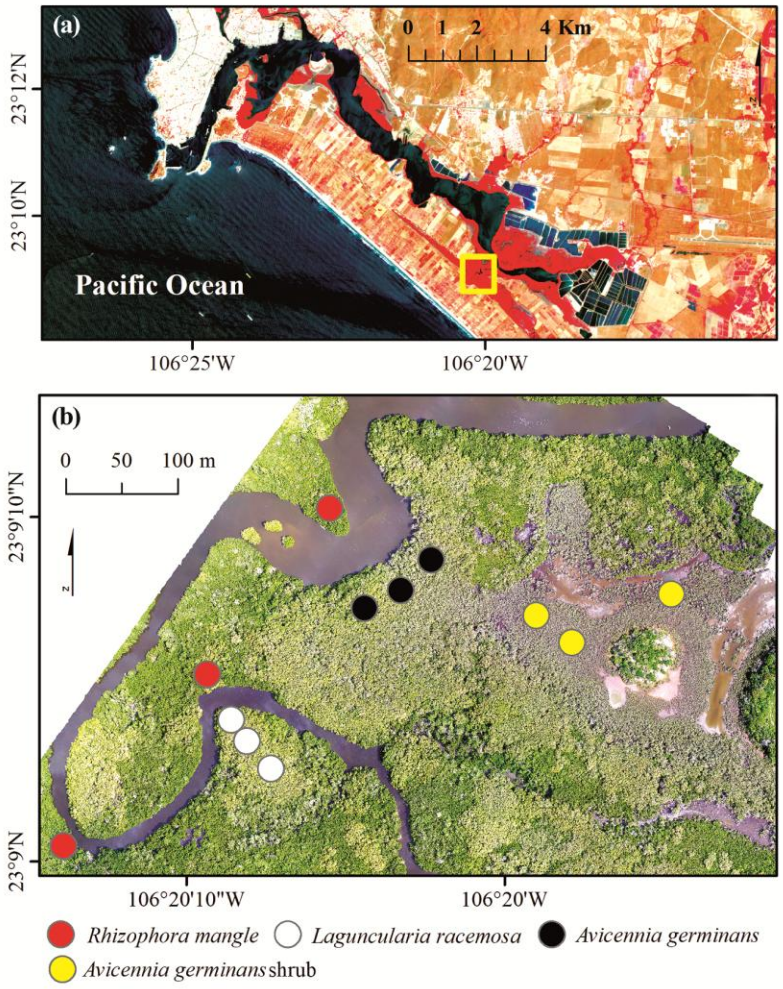

Fig. 1 — (a) Location of the Urias coastal lagoon system, Pacific coast of Mexico (Enhanced Near-Infrared, Red, and Green of GeoEye-1 dated June 2013). The yellow square indicates the location of the UAV orthomosaic; and (b) Location of the vegetation classes: *Avicennia germinans* (AG), *Laguncularia racemosa* (LR), and *Rhizophora mangle* (RM)

mangrove community dominated by three species: black mangrove (*Avicennia germinans*), white mangrove (*Laguncularia racemosa*), and red mangrove (*Rhizophora mangle*)[16]. Hydroperiod variability (flooding frequency, amplitude, and intensity) creates a distinct ecological gradient within this mangrove forest[17]. Consequently, mangroves thrive in optimal conditions in fringe zones along tidal channels, while basin areas with minimal hydroperiod support stunted shrubs under hydrological stress[18].

UAV data collection and analysis

Monthly aerial surveys were conducted from July 2018 to November 2019 using a handheld DJI Phantom-3 Professional UAV equipped with an integrated RGB camera. The 45-hectare study area was surveyed systematically using Map Pilot Pro software (v.2.0.1, iOS) to automate flight paths at 120 m altitude, maintaining 80 % longitudinal and lateral image overlap for complete photogrammetric coverage[12]. All images were acquired in RAW (8-bit radiometric resolution) during solar noon (±1 hour) to minimise shadow effects, with wind speeds verified below 10 m/s using a handheld anemometer (AcuRite 00256M) prior to each flight. The UAV´s onboard GNSS receiver and IMU recorded positioning data (logged in .csv format)[19].

Prior to analysis, individual UAV images were radiometrically calibrated using pre-flight reference targets deployed at the ground control station in the MAPIR Camera Control software. This calibration is essential for mitigating quality degradation caused by atmospheric interference, surface reflectance variability, and flight instability due to wind turbulence. Following data acquisition, the imagery was processed using Agisoft Metashape Professional to generate orthorectified products, a software package widely recognised for producing high-accuracy photogrammetric outputs. The workflow comprised three sequential stages: (1) image alignment utilising the highest option, (2) 3D mesh reconstruction with texture mapping, and (3) final orthomosaic generation at a ground sampling distance of 5.8 cm.

The photogrammetric processing began with feature matching across images using 20 distributed Ground Control Points (GCPs) with sub-meter GPS measurements. The software aligned camera positions using radiometrically calibrated imagery to compensate for illumination variations. While dense stereo-matching algorithms (particularly the height-field method), effective for aerial applications, yielded high-quality outputs, the process faced significant computational constraints, particularly in processing time and hardware demands. For orthorectification, orthographic projection was selected due to its computational efficiency, generating geographic coordinate-based orthoimages while monitoring the mean reprojection error (target threshold: < 0.5 pixels) to ensure geometric accuracy[20].

Sentinel-2 time series

The spectral analysis framework was adapted from a harmonic regression approach, transitioning from Landsat-8 to Sentinel-2 data through three key modifications: (1) geolocation of sample plots using sub-meter GPS coordinates, (2) substitution of Landsat collections with Sentinel-2 Level-2A surface reflectance data (COPERNICUS/S2), and (3) implementation of band-specific cloud masking[21]. The processing was conducted via GEE code (https://earthengine.google.com)[22], analysing bands 2 (blue), 3 (green), 4 (red), and 8 (NIR) across all available images from July 1, 2018 to November 3, 2019.

As the available bands do not consist of continuous data, the harmonic analysis was implemented to model periodic signals arising from seasonal and phenological variations[23]. This approach decomposes temporal patterns into constituent harmonics - linear combinations of sine and cosine functions[24]. The harmonic order selection and the generated noise-reduced smoothed values were optimised effectively, mitigating atmospheric artefacts and outlier effects. This approach provides noise-reduced spectral trajectories by regressing band-specific reflectance (dependent variable) against temporal harmonics and trend components[25]. Subsequently, the estimated values were utilised to derive relevant vegetation indices. The modified code can be accessed via the following link: https://code.earthengine.google.com/?scriptPath=users%2Fyajvaljo%2FEntrenamiento%3ABandasPunto.

RGB vegetation indices

RGB bands were extracted from representative locations across four mangrove classes (Fig. 2), with sampling conducted within standardised 10 m^2 square plots to enable direct UAV-spaceborne comparisons. Vegetation Indices (VI) were selected based on recently established RGB-based studies[26-28]. Four key

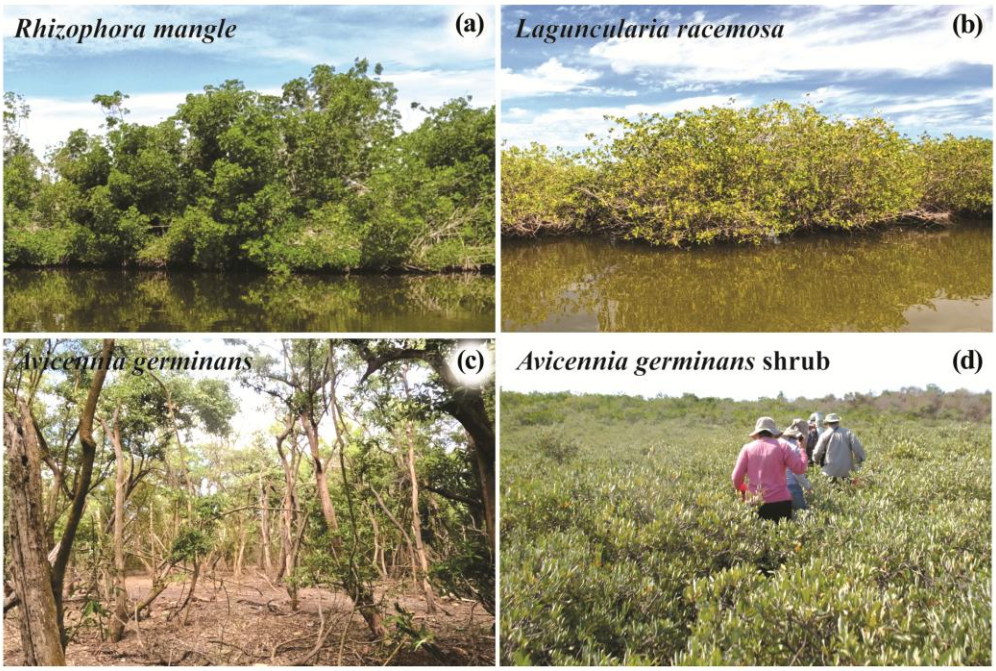

Fig. 2 — Characteristics portrayals of the vegetation classes examined for the field and remote sensing data collection: (a) *Rhizophora mangle*, (b) *Laguncularia racemosa*, (c) *Avicennia germinans*, and (d) *Avicennia germinans* shrub

Table 1 — Visible vegetation indices used in this study

Vegetation index	Equation	Reference
Visible-band Difference Vegetation Index (VDVI)	(2G-R-B)/ (2G+R+B)	Wang *et al.*[15]
Normalised Green-Red Difference Index (GRVI)	G-R/G+R	Tran *et al.*[7]
Modified Green Red Vegetation Index (MGRVI)	G^2-R^2/G^2+R^2	Bendig *et al.*[26]
Red-Green-Blue Vegetation Index (RGBVI)	G^2-(B R)/G^2+ (B R)	Bendig *et al.*[26]

*R, G, and B denote red, green, and blue data, respectively

RGB VIs were subsequently compared between UAV-derived and GEE-processed Sentinel-2 data (Table 1). Linear relationships between vegetation indices were assessed from both platforms using bivariate correlation analysis, calculating Pearson's correlation coefficient (r) for the whole trend. Bivariate correlation strength was categorised as strong ($|r| \geq 0.7$), moderate ($0.3 \leq |r| < 0.7$), or weak ($|r| < 0.3$), with statistical significance evaluated at $\alpha = 0.05$ after verifying normality (quantile-quantile plot test) and homoscedasticity.

Results

Figure 3 presents the seasonal patterns of four VIs derived from GEE data across mangrove species. All evergreen mangroves showed phenological consistency, with peak VI values occurring post-rainy season (September – December) and minima during the dry season (April – June). *Avicennia germinans* (shrub condition) consistently exhibited the lowest VI values, while *Rhizophora mangle* showed the highest. Among indices, Normalised Difference Vegetation Index (NDVI) yielded the greatest magnitude, followed sequentially by Modified Green Red Vegetation Index (MGRVI), Green Red Vegetation Index (GRVI), and Red Green Blue Vegetation Index (RGBVI).

Figure 4 displays visible-spectrum VI derived from the consumer-grade UAV camera. While VI magnitudes were systematically lower than corresponding GEE-platform values (*e.g.*, 0.3 ± 0.1 for MGRVI), both datasets captured consistent phenological patterns, including post-rainy season peaks and dry-season minima. Notably, *Avicennia germinans* (shrub condition) exhibited attenuated seasonality ($p > 0.05$). These observations align with significant bivariate correlations between UAV and GEE-derived VI (Table 2), confirming inter-platform consistency despite absolute value differences.

Discussion

This study aimed to compare monthly VI values derived from consumer-grade UAV-based RGB imagery with those obtained from the GEE platform, focusing on evergreen mangrove forests. Using field

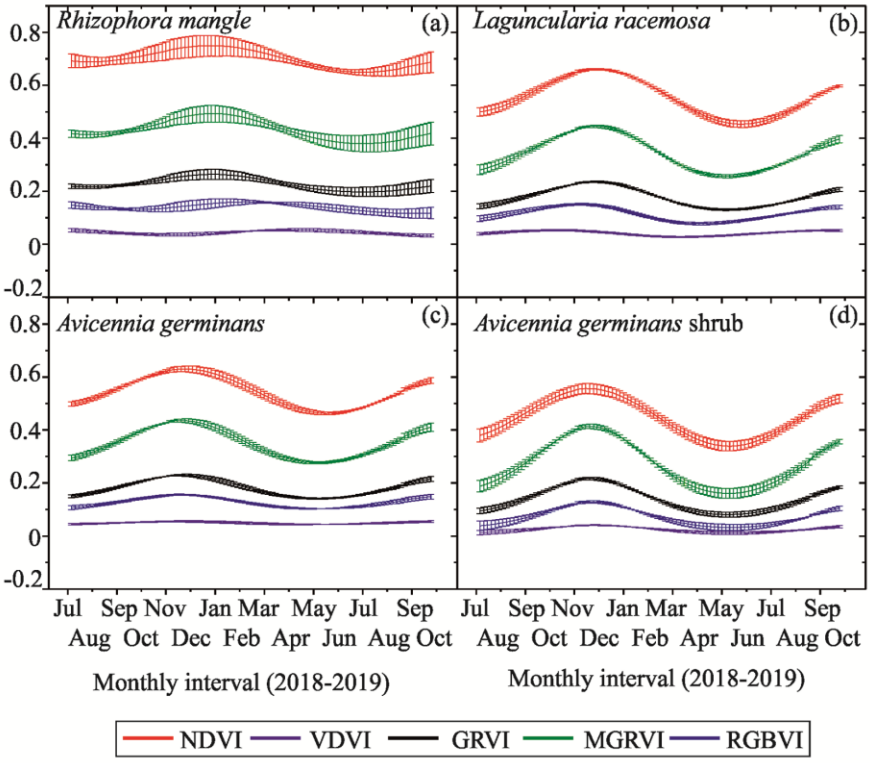

Fig. 3 — Time series of the vegetation indices profiles created by the Sentinel-2 data. Error bars are denoted for each vegetation class. Normalised Difference Vegetation Index (NDVI), Visible-band Difference Vegetation Index (VDVI), Normalised Green-Red Difference Index (NGRDI), Modified Green Red Vegetation Index (MGRVI), and Red-Green-Blue Vegetation Index (RGBVI)

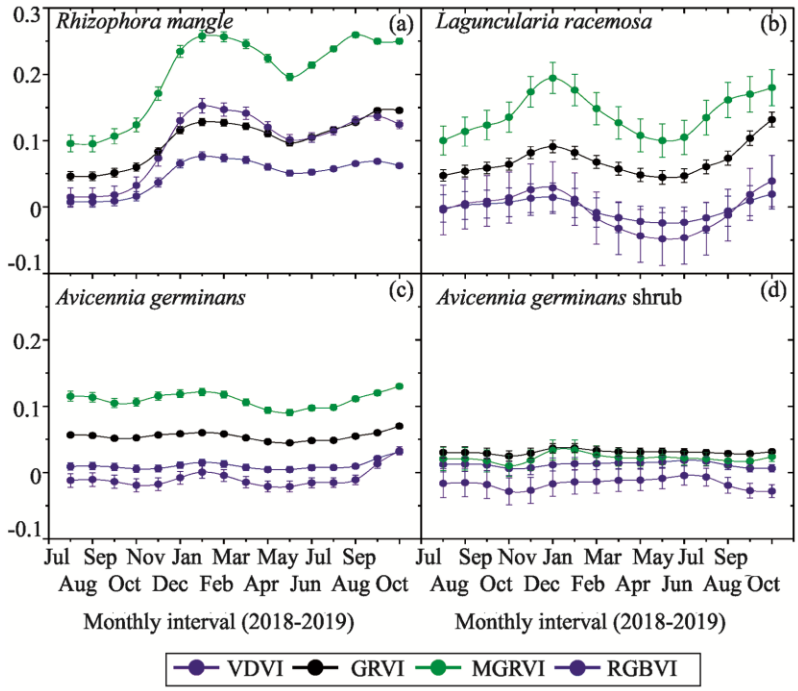

Fig. 4 — Time series of the vegetation indices profiles created by the consumer-grade UAV camera. Error bars are denoted for each vegetation class. Visible-band Difference Vegetation Index (VDVI), Normalised Green-Red Difference Index (NGRDI), Modified Green Red Vegetation Index (MGRVI), and Red-Green-Blue Vegetation Index (RGBVI)

Table 2 — Bivariate correlation analysis between the vegetation indices derived from the consumer-grade UAV camera and the Google Earth Engine platform. *Indicates significance at $p < 0.05$

Class	Vegetation index			
	MGRVI	NGRVI	VDVI	RGBVI
Rhizophora mangle	0.09	0.18	0.02	0.07
Laguncularia racemosa	0.78*	0.83*	0.53	0.72*
Avicennia germinans	0.70*	0.35	0.69*	0.70*
Avicennia germinans shrub	0.25	0.02	0.24	0.21

and remote sensing approaches, the capability of a specific VI to capture seasonal trends in subtropical mangrove trees and shrubs was assessed. A key methodological contribution was the application of radiometric correction to consumer-grade UAV images, enabling multi-temporal analysis. Although consumer-grade UAV cameras are not inherently designed for phenological monitoring, radiometric calibration facilitated the detection of similar seasonal trends in certain vegetation classes. However, the UAV-derived VI values obtained were consistently lower than those from the GEE platform.

This study delineated the phenological trajectory of local mangrove species using time-series VI, offering insights for ecologists studying mangrove physiology and ecology. The methodology could benefit the remote sensing community by enabling more accurate mapping of mangrove forests extent and condition[10]. Similar time-series VI profiles were observed by Li *et al*.[29], though the referenced study focused on *Kandelia obovata*, *Aegiceras corniculatum*, *Avicennia marina*, and *Bruguiera gymnorrhiza* in China. Sentinel-2-based NDVI time-series data demonstrated significant improvements over Landsat-based data, primarily due to its higher spatial resolution (10 m *vs*. 30 m). While Landsat provides up to 24 usable observations annually, this temporal resolution may still be insufficient to capture fine-scale phenological variation in mangrove species[22].

Assessment of mangrove species in a localised area of the Urias coastal lagoon in the current study demonstrated the potential for large-scale mangrove species mapping. However, accounting for variations in life cycle stages among species is critical[30]. Previous studies have shown that mangrove phenology is influenced by local climate, water and soil salinity, latitude, and interactions with surrounding vegetation[29]. As a result, the same species may exhibit morphological differences across distinct locations[31], highlighting the need for expert knowledge when monitoring long-term and spatially variable mangrove dynamics[18]. A key limitation of current study species identification method is the uncertainty associated with tracking these changes over large spatial and temporal scales[29].

Reliable training samples are essential for understanding image properties and developing accurate classification rules[16]. High-quality training data is essential for creating detailed classification maps[32], yet their correction poses several challenges. First, positioning systems inaccuracies may introduce location errors in training samples, leading to misclassified pixels in remotely sensed imagery[8]. Second, converting field survey points into pure pixels (single land-cover type) is often problematic[33]. For example, each training sample should ideally represent a pure pixel of at least 10 m × 10 m. However, due to the small area and high species heterogeneity of the Urias coastal lagoon, few pure 10 m × 10 m plots are available[15].

The use of UAV-derived data enabled accurate adjustment of Sentinel-2 imagery, facilitating the generation of numerous high-accuracy ground truth samples[12]. This cost-effective approach, as demonstrated by Li *et al*.[29], leverages GEE cloud computing to efficiently process and classify large volumes of Sentinel-2 data for mangrove species mapping. GEE automatically synchronised all Sentinel-2 data from the European Space Agency and seamlessly integrated them into the processing workflow[34]. Using simple scripts, GEE effectively filtered cloudy pixels and generated high-quality time-series data. By incorporating machine learning algorithms through GEE´s Application Programming Interface (API), this study could implement random forest classification on the platform[21]. Consequently, all phenology-based classification procedures can be executed efficiently in a cloud computing environment, eliminating dependence on local computing resources or external software.

The UAV-based RGB image acquisition method has additional inherent limitations. Although the images were captured with fixed exposure settings and underwent rigorous radiometric calibration, the high pixel density introduced a pronounced "salt-and-pepper" effect when aggregating values within the 10 m radius sampling areas for each class[10]. To address this issue, the study recommend supplementing UAV data with field spectroradiometer measurements for enhanced in situ validation[31]. Although restricted to visible-range detection (versus

NIR-enhanced VI), RGB VIs enable cost-effective, high-temporal-resolution health surveillance when paired with species-specific reflectance baselines. Spectroscopy reflectance data obtained with a field spectroradiometer are more complex and time-consuming than those from a UAV-mounted multispectral camera system designed for precision agriculture[28]. These instruments are not only costly but also demand substantial operational expense, particularly when deployed in challenging saline environments[29]. Future research should prioritise national phenological studies in larger mangrove systems, such as Marismas Nacionales, where hydrological modifications have occurred. Such investigations could provide critical insights into historical patterns of mangrove forest degradation.

Conclusion

This study evaluated the detection of seasonal variations using visible-spectrum vegetation indices derived from UAV-based RGB imagery. The method demonstrated strong agreement (r = 0.83) between UAV orthomosaics and spaceborne sensor data for phenological monitoring in small-scale mangrove ecosystems, presenting a cost-effective alternative to ground-based spectroscopy. While effective, the approach was constrained by long orthomosaic processing times (several hours per flight). For semiarid mangroves with distinct wet/dry seasonality, these techniques show promise in tracking species-specific physiological responses to environmental drivers. Future research should expand these methods to diverse coastal systems, ideally incorporating multispectral UAV sensors to enhance discriminatory capacity for mangrove functional traits under climate change scenarios.

Acknowledgments

FFdS acknowledges financial support for this research through grants provided by the Programa de Apoyo a Proyectos de Investigación e Inovación Tecnológica (PAPIIT grant # IA100218) and the Instituto de Ciencias del Mar y Limnología (UNAM grants #622 and #323). The RAW UAV-based data extraction was performed by Kevin Galicia-Florín.

Conflict of Interest

No potential conflict of interest was reported by the authors.

Data Availability

The data that support the findings of this study are available from the corresponding author, [FFdS], upon reasonable request.

Declaration for the Usage of AI-Assisted Tool

Grammarly Pro was employed to enhance the English language quality of the manuscript, with careful attention to retaining the original ideas.

Author Contributions

LVL: Conceptualization, data curation, methodology, visualisation, and writing–original draft preparation; FFdS: Formal analysis, writing–review & editing, amd funding acquisition; RRS: Conceptualization, data curation, software, and validation; and FFV: Investigation, supervision, and validation.

References

1 Tomlinson P B, *The Botany of Mangroves*, 2nd Edn, Vol 2, (Cambridge University Press), 2016, pp. 432. https://doi.org/10.1017/CBO9781139946575

2 Malerba M E, Duarte de Paula Costa M, Friess D A, Schuster L, Young M A, *et al*., Remote sensing for cost-effective blue carbon accounting, *Earth Sci Rev*, 238 (2023) p. 104337. https://doi.org/10.1016/j.earscirev.2023.104337

3 Rivera-Monroy V H, Lee S Y, Kristensen E & Twilley R R (eds), *Mangrove Ecosystems: A Global Biogeographic Perspective - Structure, Function, and Services*, 1st edn, (Springer Cham), 2017, pp. XVI, 399. https://doi.org/10.1007/978-3-319-62206-4

4 Muro-Torres V, Amezcua F, Ramírez-Ortiz G, Flores-de-Santiago F, Amezcua-Linares F, *et al*., Assessing the spatiotemporal relationship between coastal habitats and fish assemblages at two neotropical estuaries of the Mexican Pacific, *Diversity*, 14 (8) (2022) 1-20. https://doi.org/10.3390/d14080619

5 Ferreira A C, de Lacerda L D, Rodrigues J V M & Bezerra L E A, New contributions to mangrove rehabilitation/ restoration protocols and practices, *Wetl Ecol Manag*, 31 (1) (2023) 89-114. https://doi.org/10.1007/s11273-022-09903-2

6 Valderrama-Landeros L, Flores-de-Santiago F, Kovacs J M & Flores-Verdugo F, An assessment of commonly employed satellite-based remote sensors for mapping mangrove species in Mexico using an NDVI-based classification scheme, *Environ Monit Assess*, 190 (2018) 1-13. https://doi.org/10.1007/s10661-017-6399-z

7 Tran T V, Reef R & Zhu X, A review of spectral indices for mangrove remote sensing, *Remote Sens*, 14 (19) (2022) 1-29. https://doi.org/10.3390/rs14194868

8 Cavalli R M, Remote data for mapping and monitoring coastal phenomena and parameters: A systematic review, *Remote Sens*, 16 (3) (2024) 1-83. https://doi.org/10.3390/ rs16030446

9 Pérez-Cutillas P, Pérez-Navarro A, Conesa-García C, Zema D A & Amado-Álvarez J P, What is going on within Google

Earth Engine? A systematic review and meta-analysis, *Remote Sens Appl*, 29 (2023) p. 100907. https://doi.org/10.1016/j.rsase.2022.100907

10 Valderrama-Landeros L, Flores-Verdugo F, Rodríguez-Sobreyra R, Kovacs J M & Flores-de-Santiago F, Extrapolating canopy phenology information using Sentinel-2 data and the Google Earth Engine platform to identify the optimal dates for remotely sensed image acquisition of semiarid mangroves, *J Environ Manage*, 279 (2021) p. 111617. https://doi.org/10.1016/j.jenvman.2020.111617

11 Jia M, Wang Z, Wang C, Mao D & Zhang Y, A new vegetation index to detect periodically submerged mangrove forest using single-tide Sentinel-2 imagery, *Remote Sens*, 11 (17) (2019) p. 2043. https://doi.org/10.3390/rs11172043

12 Flores-de-Santiago F, Valderrama-Landeros L, Rodríguez-Sobreyra R & Flores-Verdugo F, Assessing the effect of flight altitude and overlap on orthoimage generation for UAV estimates of coastal wetlands, *J Coast Conserv*, 24 (3) (2020) 1-11. https://doi.org/10.1007/s11852-020-00753-9

13 Flores-de-Santiago F, Valderrama-Landeros L, Villaseñor-Aguirre J, Álvarez-Sánchez L F, Rodríguez-Sobreyra R, *et al*., Detection of beach–dune geomorphic changes by means of satellite and unmanned aerial vehicle data: The case of Altamura Island in the Gulf of California, *Coasts*, 3 (4) (2023) 383-400. https://doi.org/10.3390/coasts3040023

14 Manfreda S, McCabe M F, Miller P E, Lucas R, Madrigal V P, *et al*., On the use of unmanned aerial systems for environmental monitoring, *Remote Sens*, 10 (4) (2018) p. 641. https://doi.org/10.3390/rs10040641

15 Wang D, Wan B, Liu J, Su Y, Guo Q, *et al*., Estimating aboveground biomass of the mangrove forests on northeast Hainan Island in China using an upscaling method from field plots, UAV-LiDAR data and Sentinel-2 imagery, *Int J Appl Earth Obs Geoinf*, 85 (2020) p. 101986. https://doi.org/10.1016/j.jag.2019.101986

16 Flores-de-Santiago F & Flores-Verdugo F, A comparison of forest structural methods of semiarid mangrove species using a field-based approach, *Cienc Mar*, 50 (2024) p. e3432. https://doi.org/10.7773/cm.y2024.3432

17 Flores-Verdugo F, Ramírez-Barrón E & Flores-de-Santiago F, Hydroperiod enhancement using underground pipes for the efficient removal of hypersaline conditions in a semiarid coastal lagoon, *Cont Shelf Res*, 162 (2018) 39-47. https://doi.org/10.1016/j.csr.2018.04.008

18 Flores-de-Santiago F, Serrano D, Flores-Verdugo F & Monroy-Torres M, Application of a simple and effective method for mangrove afforestation in semiarid regions combining nonlinear models and constructed platforms, *Ecol Eng*, 103 (2017) 244-255. https://doi.org/10.1016/j.ecoleng.2017.04.008

19 Pádua L, Vanko J, Hruška J, Adao T, Sousa J J, *et al*., UAS, sensors, and data processing in agroforestry: a review towards practical applications, *Int J Remote Sens*, 38 (2017) 8-10. https://doi.org/10.1080/01431161.2017.1297548

20 Valderrama-Landeros L, Flores-de-Santiago F, Álvarez-Sánchez L F, Flores-Verdugo F & Rodríguez-Sobreyra R, The influence of spatial resolution on coastline detection by means of multisource remote sensing data, *Remote Sens Appl Soc Environ*, 35 (2024) p. 101258. https://doi.org/10.1016/j.rsase.2024.101258

21 Gorelick N, Hancher M, Dixon M, Ilyushchenko S, Thau D, *et al*., Google Earth Engine: Planetary-scale geospatial analysis for everyone, *Remote Sens Environ*, 202 (2017) 18-27. https://doi.org/10.1016/j.rse.2017.06.031

22 Chen S, Woodcock C E, Bullock E L, Arévalo P, Torchinava P, *et al*., Monitoring temperate forest degradation on Google Earth Engine using Landsat time series analysis, *Remote Sens Environ*, 265 (2021) p. 112648. https://doi.org/10.1016/j.rse.2021.112648

23 Liang J, Jin F, Zhang X & Wu H, WS4GEE: Enhancing geospatial web services and geoprocessing workflows by integrating the Google Earth Engine, *Environ Modell Software*, 161 (2023) p. 105636. https://doi.org/10.1016/j.envsoft.2023.105636

24 Shumway R H & Stoffer D S, *Time Series Analysis and Its Applications With R Examples*, 4th Edn, Vol 97, (JSTOR), 2017, pp. 325. https://www.jstor.org/stable/43298885

25 Phiri D, Simwanda M, Salekin S, Nyirenda V R, Murayama Y, *et al*., Sentinel-2 data for land cover/use mapping: A review, *Remote Sens*, 12 (14) (2020) p. 2291. https://doi.org/10.3390/rs12142291

26 Bendig J, Yu K, Aasen H, Bolten A, Bennertz S, *et al*., Combining UAV-based plant height from crop surface models, visible, and near infrared vegetation indices for biomass monitoring in barley, *Int J Appl Earth Obs Geoinf*, 39 (2015) 79-87. https://doi.org/10.1016/j.jag.2015.02.012

27 Wan L, Li Y, Cen H, Zhu J, Yin W, *et al*., Combining UAV-based vegetation indices and image classification to estimate flower number in oilseed rape, *Remote Sens*, 10 (9) (2018) p. 1484. https://doi.org/10.3390/rs10091484

28 Yeom J, Jung J, Chang A, Ashapure A, Maeda M, *et al*., Comparison of vegetation indices derived from UAV data for differentiation of tillage effects in agriculture, *Remote Sens*, 11 (13) (2019) p. 1548. https://doi.org/10.3390/rs11131548

29 Li H, Jia M, Zhang R, Ren Y & Wen X, Incorporating the plant phenological trajectory into mangrove species mapping with dense time series Sentinel-2 imagery and the Google Earth Engine platform, *Remote Sens*, 11 (21) (2019) p. 2479. https://doi.org/10.3390/rs11212479

30 Celis-Hernandez O, Villoslada-Peciña M, Ward R D, Bergamo T F, Perez-Ceballos R, *et al*., Impacts of environmental pollution on mangrove phenology: Combining remotely sensed data and generalized additive models, *Sci Total Environ*, 810 (2022) p. 152309. https://doi.org/10.1016/j.scitotenv.2021.152309

31 Flores-de-Santiago F, Kovacs J M & Flores-Verdugo F, The influence of seasonality in estimating mangrove leaf chlorophyll-a content from hyperspectral data, *Wetl Ecol Manag*, 21 (3) (2013) 193-207. https://doi.org/10.1007/s11273-013-9290-x

32 Yang G, Huang K, Sun W, Meng X, Mao D, *et al*., Enhanced mangrove vegetation index based on hyperspectral images for mapping mangrove, *ISPRS J Photogramm Remote Sens*, 189 (2022) 236-254. https://doi.org/10.1016/j.isprsjprs.2022.05.003

33 Hengl T, Finding the right pixel size, *Comput Geosci*, 32 (9) (2006) 1283-1298. https://doi.org/10.1016/j.cageo.2005.11.008

34 Mutanga O & Kumar L, Google earth engine applications, *Remote Sens*, 11 (5) (2019) p. 591. https:// doi.org/10.3390/rs11050591